Remote Sensing of Environment 164 (2015) 155–169

Contents lists available at ScienceDirect

Remote Sensing of Environment

journal homepage: www.elsevier.com/locate/rse

Snow cover variability in a forest ecotone of the Oregon Cascades via MODIS Terra products

Tihomir Sabinov Kostadinov *, Todd R. Lookingbill

Department of Geography and the Environment, 28 Westhampton Way, University of Richmond, Richmond, VA 23173, USA

ARTICLE INFO

Article history:
Received 12 June 2014
Received in revised form 31 March 2015
Accepted 3 April 2015
Available online xxxx

Keywords:
Snowmelt metrics
Depletion curves
Western hemlock-true fir ecotone
Generalized least squares regression
Trend power analysis
PDO/ENSO
Pacific Northwest

ABSTRACT

Snow cover pattern and persistence have important implications for planetary energy balance, climate sensitivity to forcings, and vegetation structure, function, and composition. Variability in snow cover within mountainous regions of the Pacific Northwest, USA is attributable to a combination of anthropogenic climate change and climate oscillations. However, snow covered areas can be heterogeneous and patchy, requiring more detailed mapping of snow trends to understand their potential influences on montane forests. We used standard daily MODIS snow products (MOD10A1.5) to investigate the 15-year record (2000–2014) of snow cover in the predominant forest ecotone of the Oregon Western Cascades. We modeled the ecotone using field data from the H.J. Andrews Experimental Forest, and only considered forested MODIS Terra pixels located within the mapped ecotone of a five-county region. Three snow cover metrics were developed using both binary and fractional snow cover data: mean ecotone snow cover percent, number of snow covered days during the melt season, and day of snow disappearance. Snow cover and depletion dates exhibited large interannual variability and no significant linear trends. This variability is likely influenced by the preceding wintertime states of the Pacific Decadal Oscillation (PDO) and the El Niño/Southern Oscillation (ENSO), which tend to covary. We improve and generalize existing methods for power analysis of trend estimation and quantify the number of uninterrupted observations of the snow metrics that would be needed to distinguish trends of different magnitudes from noise variance, taking possible autocorrelation into account. Sensitivity analyses of the results to some of our heuristic choices are conducted, and challenges associated with optical remote sensing of snow in a dense montane forest are discussed.

© 2015 The Authors. Published by Elsevier Inc. This is an open access article under the CC BY-NC-ND license (http://creativecommons.org/licenses/by-nc-nd/4.0/).

1. Introduction and background

Global increases in surface temperature have direct and indirect implications for the hydrological cycle. Anthropogenic changes in radiative forcing affect precipitation (including changes in amount, frequency, timing, and type), evaporation, and sensible heat transfer at the Earth's surface (IPCC, 2013). Even relatively small changes in temperatures can have large effects on the hydrologic cycle including alterations to soil moisture, drought, and flooding regimes (Barnett, Adam, & Lettenmaier, 2005; USGCRP, 2000). More than one-sixth of the world's population depends on glaciers or seasonal snow for their available water, and these supplies are at significant risk as a consequence of a warming climate (Barnett et al., 2005). Snowmelt runoff dominates the hydrologic cycle in mountainous regions of the western USA, where significant portions of annual precipitation fall as snow (Serreze, Clark, Armstrong, McGinnis, & Pulwarty, 1999). Although snow telemetry (SNOTEL) data provide empirical evidence for decreasing trends in snow water equivalent (SWE) within the Pacific Northwest in recent decades (Mote, 2003; Mote, Hamlet, Clark, & Lettenmaier, 2005), model projections for future changes in winter precipitation as a consequence of anthropogenic warming are more equivocal (Mote & Salathé, 2010).

Annual variability in snow can also be influenced by climate oscillation modes associated with ocean–atmosphere couplings such as the El Niño/Southern Oscillation (ENSO) and the Pacific Decadal Oscillation (PDO) (Hamlet & Lettenmaier, 2007). In the Pacific Northwest, variability in ocean circulation patterns over the last 25,000 years can explain significant variation in coastal fog and sediment transport (Briles, Whitlock, Bartlein, & Higuera, 2008; Long & Whitlock, 2002; Van Laningham, Duncan, Pisias, & Graham, 2008). Over the past two centuries, streamflow in the Columbia River has been as sensitive to these teleconnections as to the considerable water withdrawal for irrigation in the basin (Naik & Jay, 2011), and the strength of these linkages has increased in the 20th century (Gedalof, Peterson, & Mantua, 2004). The PDO and ENSO are an important source of decadal-scale climate variability throughout the Pacific Northwest (Abatzoglou, Rupp, & Mote,

* Corresponding author. Tel.: +1 804 484 1475; fax: +1 804 484 1577.
E-mail address: tkostadi@richmond.edu (T.S. Kostadinov).

http://dx.doi.org/10.1016/j.rse.2015.04.002
0034-4257/© 2015 The Authors. Published by Elsevier Inc. This is an open access article under the CC BY-NC-ND license (http://creativecommons.org/licenses/by-nc-nd/4.0/).

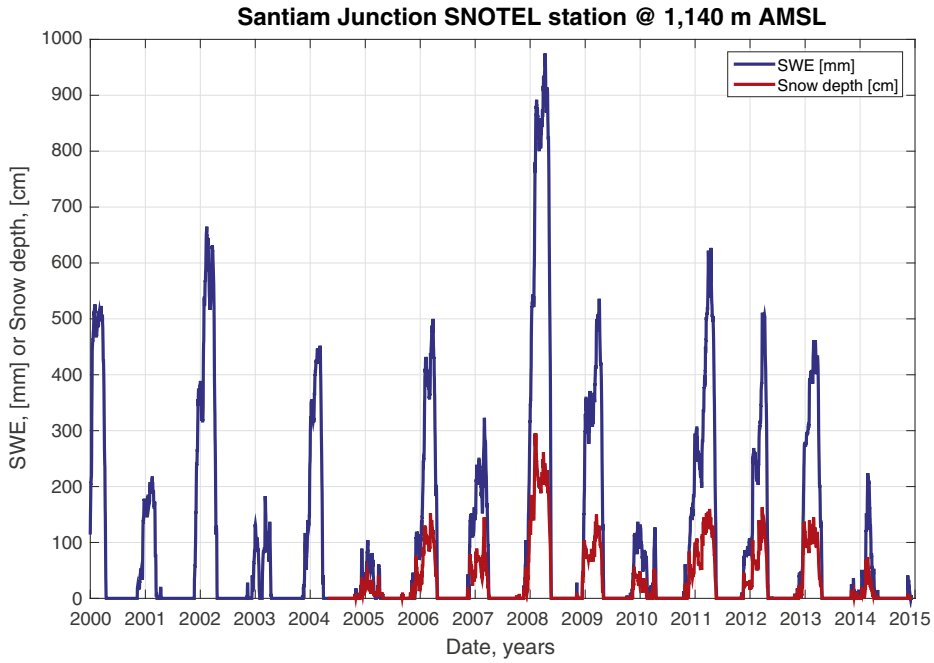

Fig. 1. Santiam Junction SNOTEL site snow water equivalent (SWE) in mm (blue curve) and snow depth in cm (red curve). See Fig. 2B or Fig. 3 for the SNOTEL station location (red diamond). AMSL = above mean sea level. (For interpretation of the references to color in this figure legend, the reader is referred to the web version of this article.)

2014; Cayan, Dettinger, Diaz, & Graham, 1998; Dettinger, Cayan, Diaz, & Meko, 1998; Wise, 2010), with warm-phase PDO and El-Niño years tending to be warmer and drier than average and cold-phase PDO and La-Niña years tending to be colder and wetter than average; these effects are generally additive and get amplified when PDO and ENSO are in phase (Climate Impacts Group, 2014a; Hamlet & Lettenmaier, 1999).

Several studies have examined the relative contributions of global climate change trends and PDO/ENSO climate oscillations to snow dynamics in the mountains of the western US and determined that both have detectable signals (Moore, Holdsworth, & Alverson, 2002; Mote, 2006; Peng, Zhongbo, & Gautam, 2013). However, these studies typically provide inferences over large regions (Trujillo & Molotch, 2014) or use changes in streamflow as the response variable of interest, which aggregates snowmelt over entire basins (e.g., Stewart, Cayan, & Dettinger, 2005). Snow covered areas can be heterogeneous and patchy, varying over very small spatial scales, especially in forested and/or complex terrain (Lundquist & Lott, 2008; Raleigh et al., 2013). Many forest processes that are dependent on snow hydrology, such as seedling recruitment and mortality, operate at these finer functional scales (Dingman et al., 2013; Mori, Mizumachi, & Sprugel, 2008). For example, snow dynamics may be a key factor influencing the specifics of forest composition change within forest community ecotones of the Pacific Northwest (Lookingbill, Rocca, & Urban, 2011; Mori et al., 2008); however, snow variability has been poorly quantified at these local scales. Existing ground-based sensor networks such as SNOTEL (Serreze et al., 1999) indicate the high annual variability of snow cover (Fig. 1), but are generally too sparsely distributed to capture the fine spatial scales required for ecotone-level studies. No studies have been published in the region using remotely sensed snow products to evaluate snow trends within a specific forest community ecotone.

Remotely sensed data can provide the daily synoptic world-wide sampling at high spatial resolution required to track seasonal changes in forest snow cover (Nolin, 2010). Standard operational snow cover algorithms for the Moderate Resolution Imaging Spectroradiometer (MODIS) sensors retrieve snow presence or absence (binary product) or fractional snow covered area (fSCA) using the visible and near-infrared (NIR) bands (Riggs, Hall, & Salomonson, 2006). Hall, Foster, DiGirolamo, and Riggs (2012) derived metrics of snow cover amount and timing of melt from ten years of MODIS data for the Wind River Range in Wyoming, USA and found a significant correlation with spring discharge in the basin. A similar approach could be used to develop ecologically relevant metrics for evaluating potential changes in snow condition at a forest community ecotone. Useful metrics would consider the relationship between the phenology of snow-tolerant species and the timing of melt (Mori et al., 2008). These metrics would allow the assessment of overall trends in snow cover and duration and the influence of PDO/ENSO climate oscillations on these trends. In addition, quantification of the inter-annual variance in snow cover metrics would allow the estimation of the record length required to distinguish statistically significant trends from noise.

Here, we use standard daily MODIS Terra binary and fSCA snow products for the 2000–2014 period to investigate snow cover variability in the western hemlock-true fir ecotone of the Oregon Western Cascades. We develop and compare three ecologically meaningful snow metrics using both data sets and map these metrics for MODIS Terra pixels located within the ecotone. We hypothesize that the annual variability in the metrics is associated with the state of the PDO and ENSO. To test this hypothesis, we divide the time series into wintertime warm, cold and neutral PDO/ENSO years and compare the snow metrics for the cold vs. the warm years using Wilcoxon rank-sum tests. We also investigate the linear correlation of PDO/ENSO indices with our metrics. We test for the presence of linear trends for the fifteen years of data and quantify noise variance in the data; we then generalize existing power analysis of trend estimation methods and use them to forecast the minimum length of record that would be required to detect long-term changes in snow cover for this ecotone.

2. Study area

2.1. Geographic setting

The study area comprises the Oregon Western Cascades within Clackamas, Marion, Linn, Lane and Douglas counties, eastwards of 123°7′40″W (Fig. 2). These counties were chosen because their

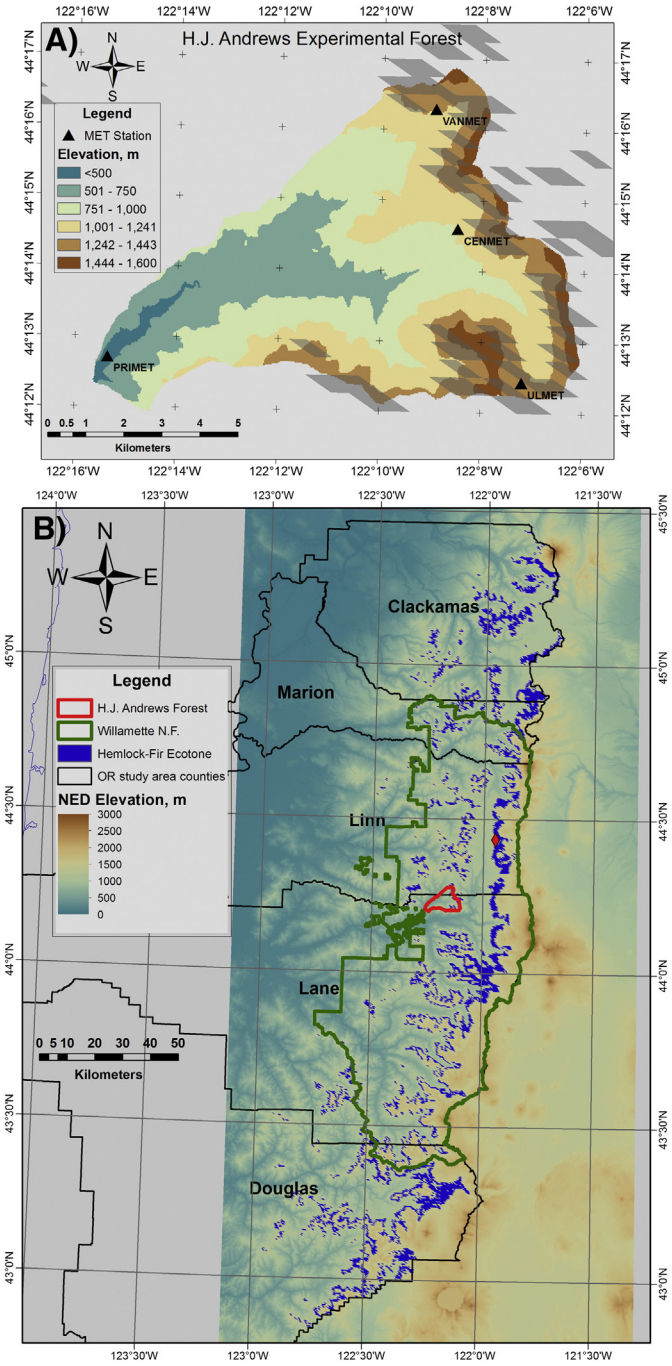

Fig. 2. (A) Elevation map (from NED data) of the H.J. Andrews Experimental Forest (HJA). The beige-colored 1242–1443 m band illustrates the elevation range of the hemlock-fir ecotone. MODIS pixels from the MOD10A1.5 data set (500 m resolution in sinusoidal projection, tile h09v04) that belong to the ecotone are shaded in light gray and overlaid on the map. The locations of four main meteorological stations are shown for reference. (B) Map of the entire western hemlock-true fir ecotone included in this study, superimposed on an elevation map of the region. MODIS pixels from the MOD10A1.5 data set (as in (A)) belonging to the ecotone are shown in dark blue. The location of the Santiam Junction SNOTEL station is shown as a red diamond. The map datum for both maps is NAD83 HARN and the projection is Oregon-centered Lambert conformal conic. (For interpretation of the references to color in this figure legend, the reader is referred to the web version of this article.)

boundaries follow the ridge of the Western Cascade Mountains in the roughly N–S direction. The western hemlock-true fir ecotone is extrapolated using data from the H.J. Andrews Experimental Forest Long Term Ecological Research site (HJA, Fig. 2A, also shown as a red outline straddling Linn and Lane counties in Fig. 2B); therefore the study area is limited to parts of the Western Cascades that are reasonably close to the HJA. The Cascade Range within the five study counties is located within less than ~1.5° latitude (~170 km) N or S of the HJA. The majority of the study area is contained within the Willamette National Forest.

2.2. Mapping the western hemlock-true fir ecotone

The spatial transition from western hemlock (*Tsuga heterophylla*) to true fir (*Abies amabilis* and *Abies procera*) community association is the dominant forest ecotone in the Western Cascade Mountains. The ecotone was modeled for the study region, based on a classification and regression tree (CART) analysis conducted in the HJA (Lookingbill & Urban, 2005). Here, we simplified the criteria to use only the elevation-based branches of the CART model in order to classify MODIS pixels from tile h09v04 (sinusoidal projection, 500 m nominal

resolution) of the MOD10A1.5 snow cover data set (Section 3.1) as either belonging to the ecotone or not belonging to it. Subsequent analyses are carried out only for the ecotone pixels. Elevation was derived from the 1-arcsecond (~30 m) USGS National Elevation Dataset (NED) (Gesch, 2007; Gesch et al., 2002), available at http://ned.usgs.gov. The mean elevation of each MODIS pixel was determined using zonal statistics (provided by ESRI's ArcGIS®) over the ~256 NED pixels covering a single MODIS pixel. MODIS pixels were classified as belonging to the ecotone if they had mean NED elevation between 1242 and 1443 m, inclusive, as this is the elevation band of the ecotone as modeled by Lookingbill and Urban (2005) (Fig. 2).

The dynamics of snow accumulation and melt differ considerably for different land covers. Because of the large differences between forests and fields, we included only forested pixels in our analysis. The National Land Cover Dataset (NLCD 2006) (Fry et al., 2011), was used to determine which MODIS pixels could be classified as evergreen forest (~256 NLCD pixels per MODIS pixel). A MODIS pixel was considered to be part of the ecotone only if it was at least 80% evergreen forest (Class #42 in the NLCD 2006 data set). The MODIS snow cover tile h09v04 is 2400 × 2400 pixels (1200 × 1200 km), out of which 7437 pixels (~0.13% of the tile) were classified as belonging to the ecotone (Fig. 2B). The total area of these MODIS ecotone pixels is approximately 1600 km^2. The ecotone map is provided in ESRI® ASCII and Geotiff raster formats as *Supplementary data* to this article (see link in Appendix B).

In summary, MODIS pixels are considered to be ecotone pixels (Fig. 2B) if all of the following conditions are met: 1) elevation between 1242 and 1443 m; 2) within the boundaries of the following five Oregon counties: Clackamas, Marion, Linn, Lane and Douglas; 3) at least 80% covered by evergreen forest; and 4) part of tile h09v04 of the MODIS snow cover data set MOD10A1.5 (Section 3.1).

3. Data and methods

3.1. Snow cover data

Daily MODIS Terra snow cover maps for the period February 24, 2000–November 10, 2014 were obtained from the National Snow and Ice Data Center (NSIDC), at http://www.nsidc.org. Data from the product MOD10A1.5 (Hall & Riggs, 2007; Hall, Salomonson, & Riggs, 2006; Riggs et al., 2006), tile h09v04 were used to create snow cover depletion curves specific to the modeled ecotone only. MOD10A1.5 contains binary daily snow cover (snow or no snow) and continuous fractional snow covered area (fSCA) at 500 m resolution, in sinusoidal projection. The binary retrieval for MODIS Terra is based on a threshold test on the normalized difference snow index (NDSI), calculated from bands 4 (0.545–0.565 μm) and 6 (1.628–1.652 μm); many additional threshold tests are also used (Hall, Riggs, & Salomonson, 2001; Riggs et al., 2006). Details of the algorithm are provided in Hall et al. (2001), Riggs et al. (2006) and Hall and Riggs (2007). fSCA is calculated from empirical linear relationships with true sub-pixel snow cover from Landsat data (Hall & Riggs, 2007; Salomonson & Appel, 2004). The binary and fSCA data sets are used here for independent, parallel analyses. Example binary and fSCA US Pacific Northwest snow cover maps for January 27, 2012 are shown in Fig. 3. The sinusoidal projection has the advantage of being equal area, so any spatial statistics need no corrections. MODIS snow cover data were analyzed as is, resampling the rest of the data sets used in order to avoid any resampling of the NSIDC products. Only ecotone pixels of good data quality (quality flag = 0 in the Spatial QA data set) were used in the analysis. MODIS Terra was chosen for the analysis over MODIS Aqua because a channel failure on Aqua prevented the algorithm correction for densely-forested areas (Klein, Hall, & Riggs, 1998) to be applied; since the ecotone is a dense evergreen forest, this correction is very important and is applied to Terra data (Hall & Riggs, 2007).

Snow water equivalent (SWE) and snow depth data from the Santiam Junction SNOTEL station (elevation 1140 m) were obtained from the National Water and Climate Center and were used for comparison purposes to illustrate interannual variability in snow cover for an area close to the HJA and similar to the ecotone in elevation.

3.1.1. Cloud gap filling

Before any further processing was applied, daily imagery was cloud gap filled using the methodology of Hall, Riggs, Foster, and Kumar (2010). For cloud gap filling purposes, pixels from the MOD10A1.5 binary snow cover product classified as cloud, snow, no snow, lake, lake ice or ocean were considered valid. Pixels from the fSCA data classified as cloud, fractional snow cover (0–100%), land (none occur in actual images), inland water or ocean were considered valid. All other pixel classification values were considered invalid. Pixels that were invalid or classified as cloud were gap filled by using the most recent corresponding observation from up to three days prior to the current image's date. The gap filling was performed using a computationally efficient algorithm whereby all valid pixels of the current image and the three previous days were assigned a binary '1', and all invalid and cloudy ones were assigned a binary '0'. A 4-bit binary number was constructed for each pixel from the 4 days of observations. The most significant digit of the binary number was formed from the current day's image, the second — from one day prior, the third — from two days prior, and the least significant digit — from the image three days prior. The value of this binary number was used to determine the index of the most recent valid non-cloudy observation at each pixel. The composite cloud gap-filled image was then constructed from the four input images using these indices. For example, if the resulting binary number at a particular pixel was '0101', this indicated that the current day's image had a cloudy or invalid observation, and the most recent valid non-cloudy observation came from one day prior. Thus, the pixel value from the image one day prior was assigned to the corresponding pixel of the current day's image. Under this scheme, pixels still classified as cloud after cloud gap-filling indicate that the current day was cloudy and no valid non-cloud observations were made in any of the previous days.

3.2. Snow cover and snowmelt metrics

Snow cover time series specific to the ecotone were constructed for every year from 2000 to 2014. For metric calculation, pixels from the cloud gap-filled data classified as cloud, snow, no snow, or fractional snow cover (0–100%) were considered valid; all other pixel classification values were considered invalid. The percent snow covered pixels (out of all valid ecotone pixels) from the cloud gap-filled binary data and the mean fSCA from the cloud gap-filled fSCA data over all valid ecotone pixels were calculated for each day. Days when more than 80% of the ecotone pixels were cloud covered (even after temporal cloud-gap filling, Section 3.1.1) were considered too cloudy for analysis and were not included in the snow depletion curves (Hall et al., 2010). In addition, daily MOD10A1.5 tiles for which less than 25% of the ecotone pixels were valid were excluded from the analysis. These criteria and satellite data outages led to some days with missing data; thus before metric calculation the time series of spatially aggregated ecotone percent snow cover was temporally gap-filled using linear interpolation. This step is distinct from the cloud gap filling (Section 3.1.1) which is conducted on a per-pixel basis.

Three metrics were calculated from the snow cover time series and employed to assess snow cover dynamics in the ecotone during the snowmelt season, considered to be days of year 80 through 181 (March 20 or 21 to June 29 or 30) (Hall et al., 2012). The *first metric* was the *mean ecotone percent snow cover* over the snowmelt season, calculated by averaging the cloud gap filled and interpolated daily binary

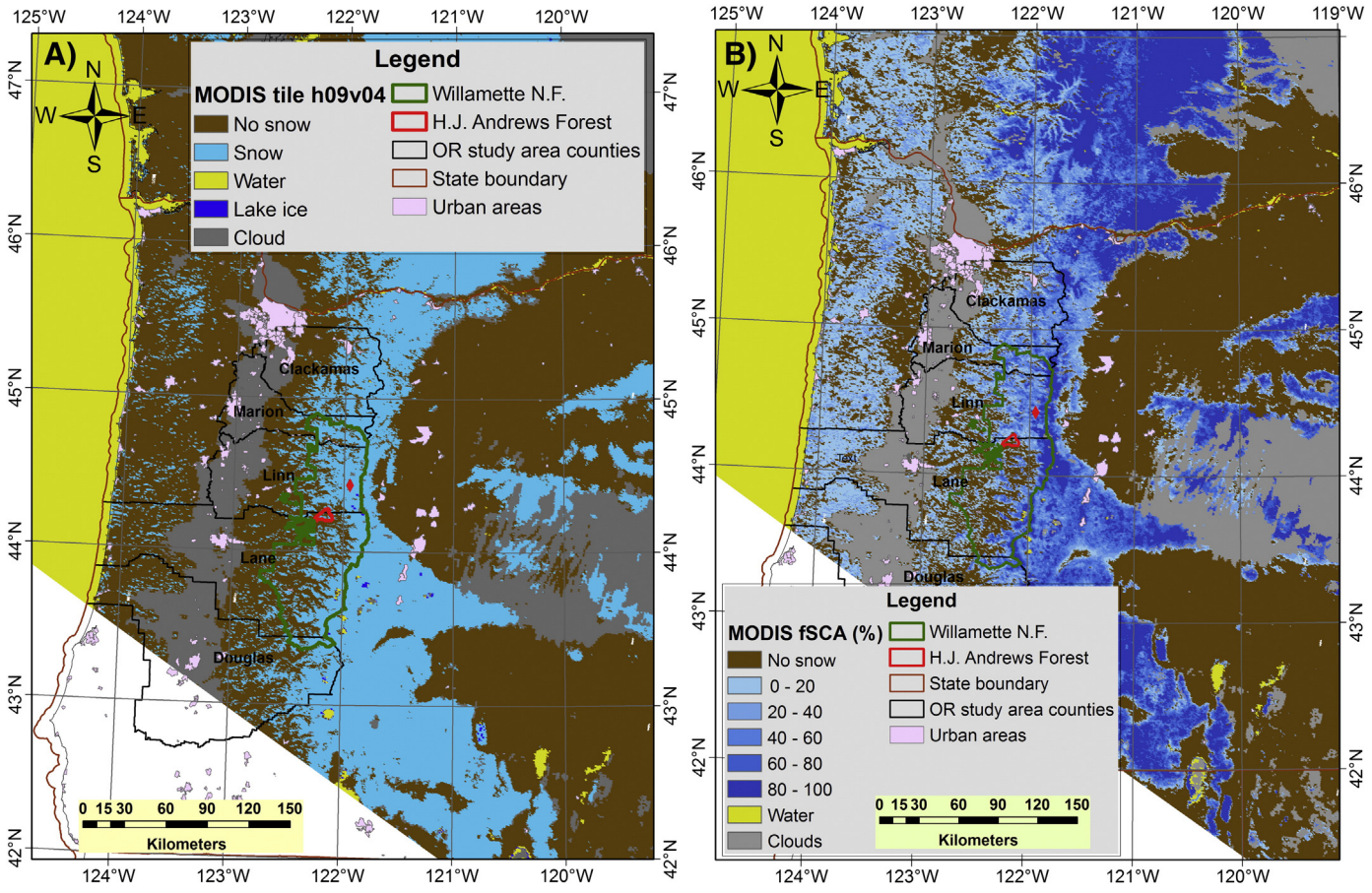

Fig. 3. (A) Example of MODIS Terra binary snow cover data for the Pacific Northwest USA from sinusoidal projection tile h09v04 of the MOD10A1.5 data set for January 27, 2012 (500 m nominal resolution). Cyan colored pixels indicate presence of snow; other pixels are color-coded as in the legend. (B) Same as in (A) but for the fractional snow cover (fSCA) data. The map datum and projection are as in Fig. 2. (For interpretation of the references to color in this figure legend, the reader is referred to the web version of this article.)

or fSCA percent snow cover. The *second metric* was the *number of snow covered days*, defined as days during the snowmelt season when snow cover was at least 20% of the valid ecotone pixels (Hall et al., 2010, 2012), also derived from both binary and fSCA data.

The *third metric* was the *day of snow disappearance*, defined as the date at which snow cover declined to less than 20% of the ecotone permanently for the season (Hall et al., 2010, 2012). Detecting the day of snow disappearance was confounded by the existence of "spikes" in the snow depletion curves, i.e. snow is first depleted to below 20% coverage and then increases to more than 20% on some subsequent days. This could be due to a late season snow storm, or it could be an algorithm or data availability artifact. There are several years in which spikes are present in the binary data (and less in the fSCA data). In those cases, we extended the day of disappearance to include the spikes only if they were within the snowmelt period considered (days 80–181) and if they were separated by less than 15 days from the preceding snow presence (>20%) condition.

3.3. Climate indices

In order to test the hypothesis that climate teleconnections due to the El Niño/Southern Oscillation (ENSO) and the Pacific Decadal Oscillation (PDO) are drivers of snow cover variability in the ecotone during the melt season, monthly values for the Multivariate ENSO index (MEI) (Wolter & Timlin, 1993, 1998) and the PDO index (Mantua, Hare, Zhang, Wallace, & Francis, 1997; Zhang, Wallace, & Battisti, 1997) were obtained for the 1995–2014 period from http://www.esrl.noaa.gov/psd/enso/mei/ and http://jisao.washington.edu/pdo/PDO.latest, respectively. The MEI index is a quantification of ENSO based on the first principal component of several meteorological variables observed over the tropical Pacific, namely sea-level pressure, vector surface winds, seas surface temperature, surface air temperature, and cloudiness fraction (Wolter, 1987; Wolter & Timlin, 1993). The PDO index is computed as the first principal component of Pacific sea surface temperature north of 20°N (Mantua et al., 1997). Monthly climate index data were smoothed using an equiripple lowpass FIR filter of order N = 18, and a pass-band frequency of 1 year^{-1} for the MEI and ½ year^{-1} for the PDO. Stop-band frequencies were set to twice the pass-band frequency. Time-lag of the filter was corrected by shifting the filtered data set by 9 months (half the filter order); this makes the filter non-causal but preserves timing of peaks and troughs in the original data.

The MEI and the PDO signals are positively correlated ($\rho = 0.63$, $p < 0.001$ for the filtered signals, $\rho = 0.60$, $p < 0.001$ for the unfiltered signals, Fig. 4), and their climate effects in the Pacific Northwest are additive (Climate Impacts Group, 2014a; Hamlet & Lettenmaier, 1999). The mean of the filtered values of the MEI for December of the preceding year to February of the current year was used to rank the years in the 2000–2014 period from coldest to warmest. Similarly, the mean of the filtered values of the PDO for October of the preceding year to March of the current year was also used to rank the same years. Since the MEI and the PDO signals are positively correlated, the mean of the two ranks was used to classify the years as being warm winter years (2003, 2004, 2005, 2007 and 2010), cold winter years (2000, 2008, 2009, 2011 and 2012), or neutral years (2001, 2002, 2006, 2013 and 2014). This classification closely matches (but is not identical to)

the classification of the Climate Impacts Group at the University of Washington (Climate Impacts Group, 2014b, their Table 1; see also Gershunov, Barnett, & Cayan, 1999), which uses different criteria.

3.4. Statistical analyses

Ecotone snow cover variability during the melt season was investigated by examining the snow cover metrics (Section 3.2) from two different perspectives. First, we tested for the presence of a linear trend in the metric time series across the 15 years of data, possibly indicating the presence of a longer-term process influencing spring-time snow cover dynamics in the ecotone. Trends were assessed via a generalized least squares (GLS) regression model accounting for possible autocorrelation of the residuals (GLS details are provided in Appendix A.1). Significance of the autocorrelation was tested using a Durbin–Watson test on the residuals. Because the MODIS record length was not expected to be long enough to detect climate-relevant trends, our main objective was to forecast the actual length of record required to distinguish a statistically significant trend from noise, accounting for autocorrelation and for both type I and type II errors. This analysis is termed power analysis of trend estimation and its details are given in Appendix A.2.

Second, we investigated the influence of PDO and ENSO climate oscillations on snow cover variability by 1) testing whether the medians of the metrics differed significantly in warm vs. cold PDO/ENSO years, using the Wilcoxon rank sum test, and 2) relating the snow cover metrics to the PDO and ENSO climate oscillation indices used to classify the years, using type I ordinary least squares (OLS) regressions.

The sensitivity of the snow cover metric trends and cold-warm years median differences to the chosen melt season start and end dates (day of year 80–181, Hall et al., 2012) was examined. These start and end dates were both varied and the effect on the magnitude and significance of the statistics was assessed. An example of a similar sensitivity analysis can be found in Fay and McKinley (2013). The melt start date was varied from day of year 45 to day of year 115 (February 14 to April 25 for common years), and the season end date was varied from day of year 130 to 212 (May 10 to July 31).

The sensitivity of the statistics calculated from the day of snow disappearance to spikes in the snow depletion curves was also investigated. All possible snow disappearance dates for each year were considered, including or excluding spikes within days of year 80–181. This led to a large number of different possible time series cases containing different combinations of snow melt dates from each year. These time series cases form the Cartesian product of the 15 sets consisting of all possible disappearance dates for each year. This 15-fold Cartesian product contained ~ one million elements for binary data and ~1.5 million elements for fSCA data. The trend and the PDO/ENSO-based statistics were calculated for all those cases and their variability and significance were evaluated.

4. Results and discussion

4.1. Melt season snow cover variability in the western hemlock-true fir ecotone

Example MODIS-based snow cover time series curves illustrate the significant interannual variability in the ecotone: the warm PDO/ENSO year 2003 (Fig. 5A) exhibited less snow cover throughout the year and somewhat earlier snowmelt, as compared to the cold PDO/ENSO year 2008 (Fig. 5B). The fSCA-based metrics consistently estimated less snow cover as compared to the binary-based metrics. In spite of cloud-gap filling, significant wintertime cloudiness in the region caused some days to not be observable via visible and NIR remote sensing. Finally, significant amount of noise in the snow curves was evident, e.g. frequent spikes occur in the data.

The observations stemming from a comparison of these two individual years (Fig. 5) were consistent with the patterns of snow cover within the ecotone for the entire MODIS Terra mission (Fig. 6). As expected for a marine west coast climate area (e.g. Christopherson, 2012), July, August and September tended to be fairly clear, whereas the rest of the year was quite cloudy, which impedes satellite-based snow studies that rely on visible and NIR wavelengths, such as the MODIS products analyzed here. The cloud gap filling improved data coverage significantly (not shown), leaving relatively few data gaps with snowmelt season days more than 80% cloud covered (Fig. 6A). A very small percentage of these gaps were due to missing data days in the MODIS record. The data gaps were filled using linear interpolation, resulting in a continuous time series of percent snow cover (Fig. 6B–C) used in the computation of the snow cover metrics (Section 3.2).

Time series of the three ecotone snow cover metrics are shown in Fig. 7A–C. The curves provide biophysically meaningful quantification

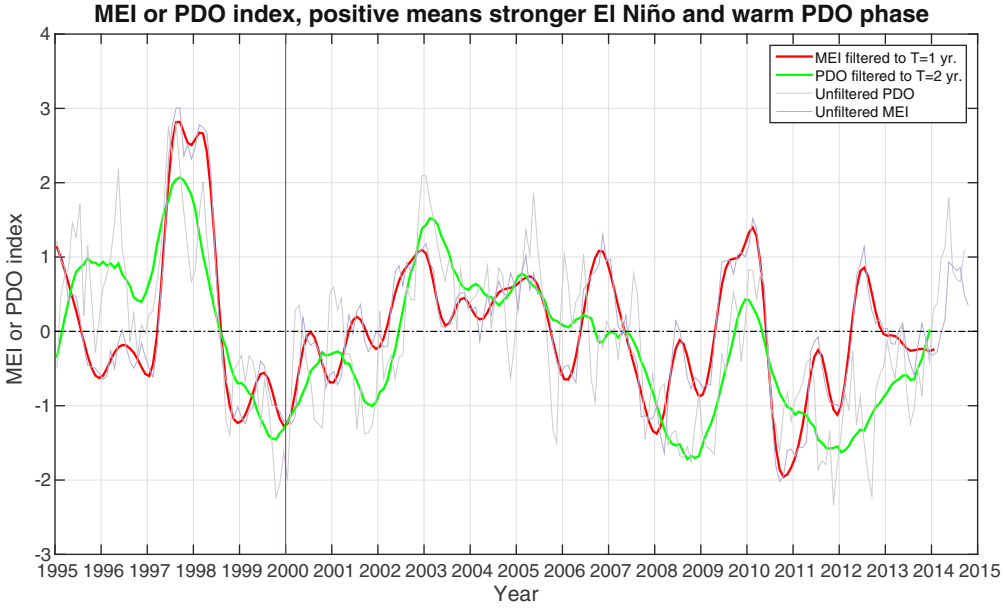

Fig. 4. Lowpass filtered and original MEI and PDO indices from 1995 to the present. The strong 1997–1998 El-Niño is evident, exhibiting the largest absolute values of the MEI and PDO signals of the entire 1995–2014 period.

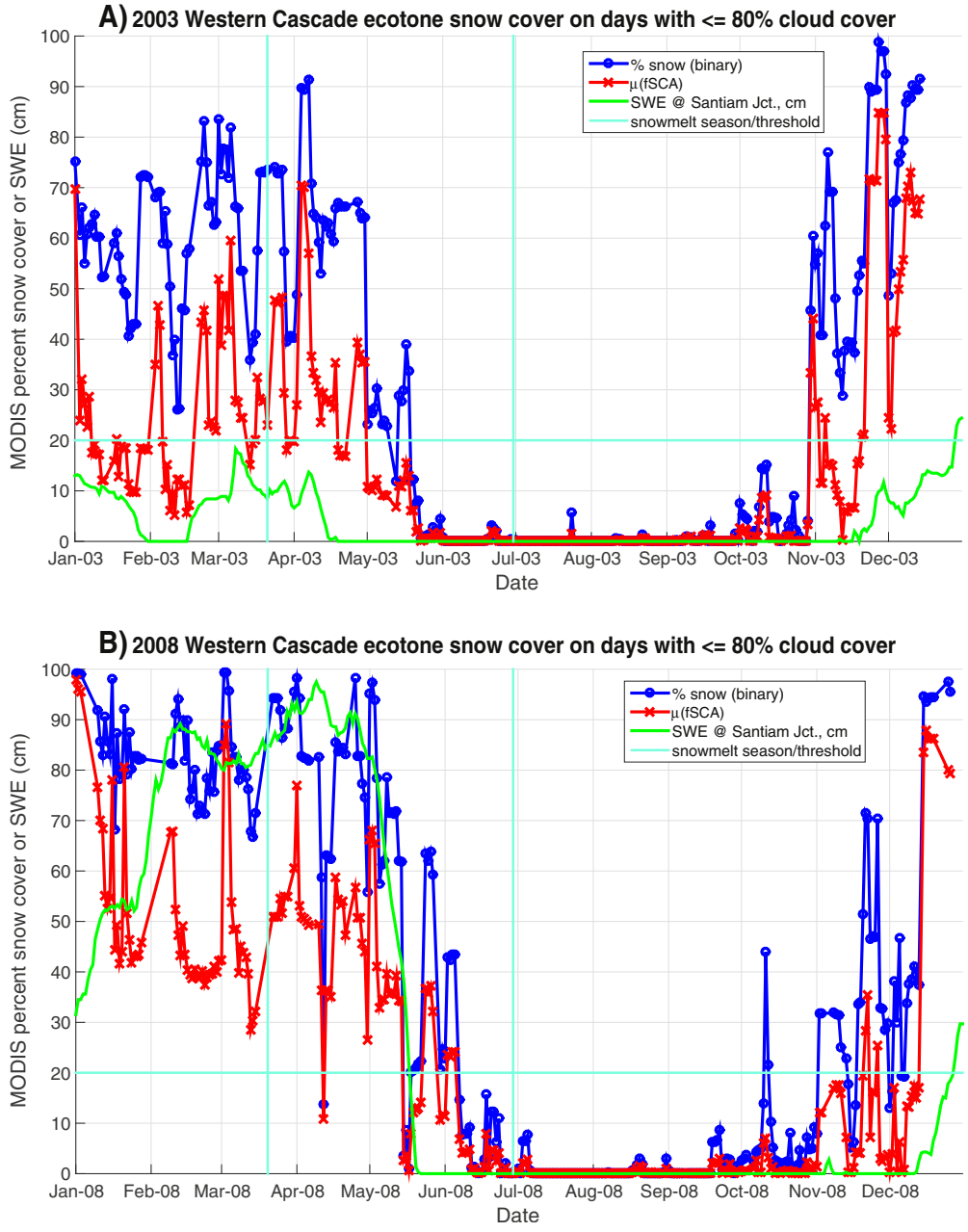

Fig. 5. (A) 2003 and (B) 2008 examples of MODIS snow cover time series for the hemlock-fir ecotone. Binary snow cover data are shown in blue; fractional snow covered area data (fSCA) are shown in red. The 20% snow cover threshold (horizontal cyan line) is used to decide whether the ecotone is snow covered or not on a given day and for determining the day of snow disappearance. Ground-based SWE data for the Santiam Junction SNOTEL station are shown in green for comparative purposes (units of cm on the same y axis as snow cover percentage). Analysis is focused on the snow cover depletion curves during the snowmelt season, days of year 80 to 181 (Hall et al., 2012), indicated by the vertical cyan lines. (For interpretation of the references to color in this figure legend, the reader is referred to the web version of this article.)

of interannual snow dynamics at the ecotone. Linear trends were not significant for any of these six time series ($R^2 < 0.1$ and all slope confidence intervals crossed zero, not shown). The Durbin–Watson test on the residuals indicated that no lag-1 autocorrelation was present in the data ($p > 0.05$). Interannual variability was high, as indicated by the standard deviation of the noise, σ_N. Quantification of autocorrelation and noise levels is critical for the power analysis of trend detection, results of which are presented in Section 4.2.

A negative trend in the time series may be expected due to a long-term interdecadal global warming signal (Mote & Salathé, 2010). However, it is not surprising that a robust long-term signal cannot be distinguished from PDO/ENSO effects and other sources of variability over this time period. We next test the hypothesis that the states of the PDO and ENSO were correlated with snow cover variability. For all three metrics and both the fSCA and binary data, the cold-phase years were consistently characterized by greater snow cover than the warm-phase years of the PDO and ENSO oscillations, as quantified by median differences (Table 1). These differences were not significant, except for fSCA-based day of snowmelt; however, the small sample size of only five years in each category makes it difficult to distinguish statistically significant median differences from random noise. OLS regressions of the snow cover metrics on the mean Oct–Mar PDO and the mean Dec–Feb MEI exhibited negative slopes (not shown), suggesting that a warmer PDO and ENSO winter leads to less overall snow cover, fewer number of snow covered days and earlier snowmelt the following spring. However, these regressions were also not significant ($p \geq 0.05$), with lots of

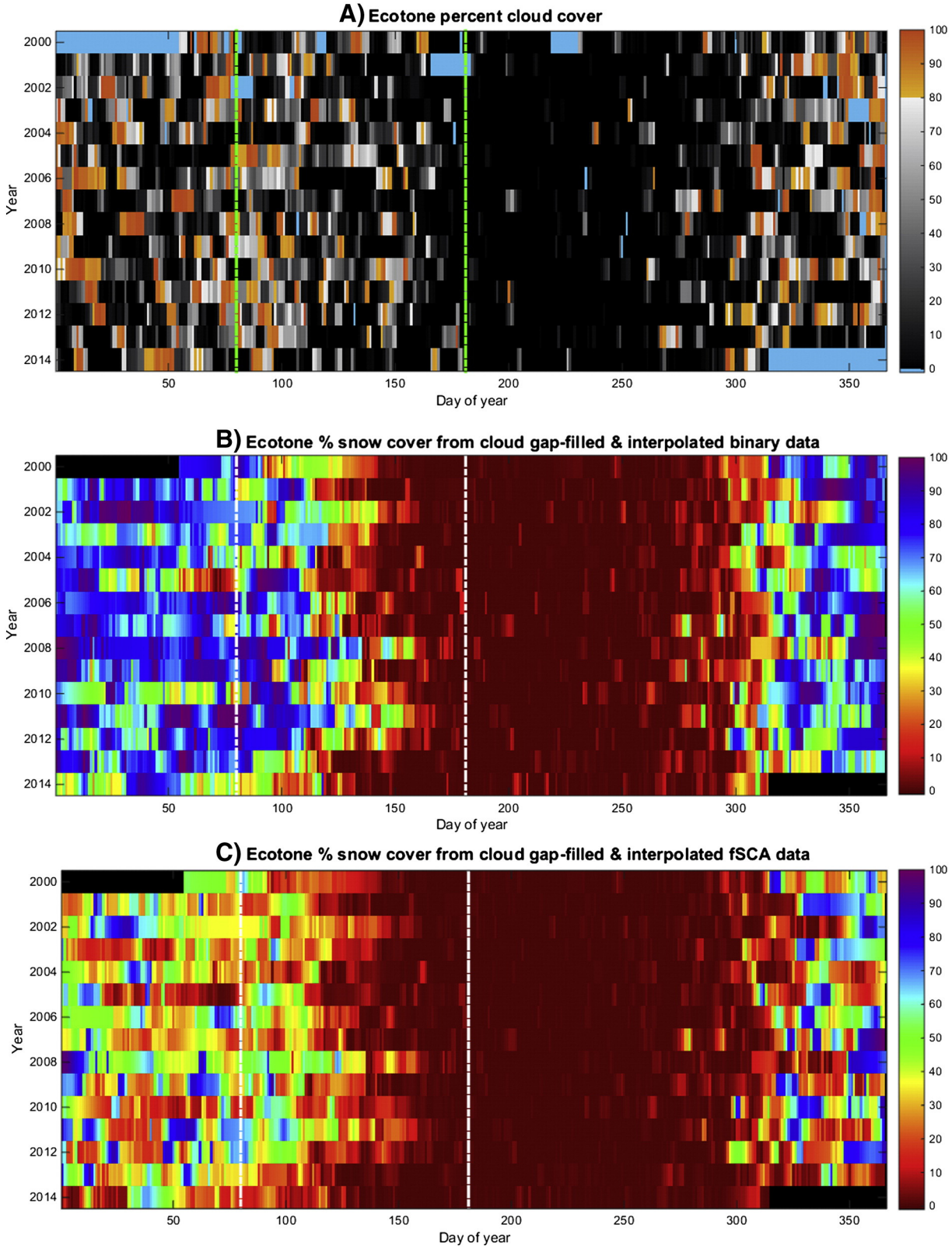

Fig. 6. (A) Percent cloud coverage over the ecotone pixels for the entire MODIS Terra mission (until Nov. 2014), after the cloud-gap filling procedure was applied (Sect. 3.1.1). The color scale indicates the percentage of valid pixels over the ecotone that were cloud covered for that day. Days with no valid data are indicated in cyan. The snowmelt season as used in the analysis here (day of year 80 to 181) is indicated with green vertical dash-dot lines in this panel and white vertical dash-dot lines in subsequent panels. (B) Percent snow cover from cloud gap-filled MODIS binary data for the modeled western hemlock-true fir ecotone. In addition to the cloud gap-filling, linear interpolation was used on the spatially aggregated daily ecotone data to fill in cloud-covered (>80%) and missing data days. (C) Same as in (B), but using the fractional snow covered area (fSCA) MODIS data. The mean fSCA over all valid ecotone pixels is shown in percent (colorbar), unless cloud cover exceeded 80%, in which case interpolation from neighboring days was used, as above. (For interpretation of the references to color in this figure legend, the reader is referred to the web version of this article.)

noise variance (low R^2 values, ranging from 0.09 to 0.26). This finding is in general agreement with the assessment that only about 30% of the variability of Pacific Northwest overall winter climate can be explained by ENSO and PDO variability (Climate Impacts Group, 2014a).

4.2. Power analysis of snow metrics trend detection

Satellite records of geophysical variables are generally too short to discern small long-term trends in noisy data (e.g. Beaulieu et al., 2013). Therefore, a major goal of trend analysis in climate change research should be the estimation of the minimal record length required to distinguish a long-term trend (possibly due to climate change) from stochastic noise or, for example, from variability caused by the PDO and ENSO oscillations. To address this question, we adapted and generalized the power analysis technique of Tiao et al. (1990) and Weatherhead et al. (1998) (Appendix A.2). The equations provided allow for the presence of first-order autocorrelation; however, since our time series did not exhibit significant autocorrelation, we set $\phi = 0$.

Results of the power analysis indicate that at the observed noise levels, a minimum of ~30 years of continuous observations would be required to distinguish a trend of about ± 0.5%/year in the percent snow cover metric (Fig. 8A), a trend of ± 1 day/year in the number of snow covered days metric (Fig. 8B) and a trend of ± 1 day/year in the day of snow disappearance metric (Fig. 8C). These example trends are quite large, leading to drastic increases or decreases in snow cover in just a few decades, assuming linear trends continue in the future. Clearly, no such assumption is warranted, but it is likely that any underlying longer-term climate change signal is smaller than these values, leading to many more years required to detect it (the gradient of T^* is very large in the x-direction as the trend magnitude tends to 0).

An alternative application of the power analysis is to assess the minimal trend (in absolute value) that can be detected given a set record length. Then, if a trend is not observed in the data, this is an indication that a trend larger than that value is not present, but a smaller possibly undetected trend may still exist. Following the 15-year contours in Fig. 8 to the observed noise level from the data in our case indicates that trends larger than ~1.3%/year (fSCA) and ~2.1%/year (binary) do not exist over this time period in the percent snow cover metric (Fig. 8A); trends larger than ~2.5–3 days/year do not exist in the number of snow covered days metric (Fig. 8B) and the day of snow disappearance metric (Fig. 8C). Otherwise such trends would have been detected under the probability assumptions of the power analysis.

4.3. Sensitivity to depletion curve spikes and the choice of snowmelt season start and end dates

The third metric (snow disappearance day) is particularly sensitive to the existence of spikes in the snow depletion curves (Fig. 5). Sensitivity analysis of all possible time series (counting or not counting spikes within the days of year 80–181 of each of the 15 years) indicated that the GLS linear trends of snow disappearance day remained insignificant in ~97% (binary-based) and ~100% (fSCA-based) of the cases tested. The Wilcoxon rank-sum tests on the median cold to warm PDO/ESNO year differences were significant in ~9% (binary) and ~49% (fSCA) of the cases, respectively, and indicated later snowmelt during cold years in 97% (binary) and 100% (fSCA) of the cases. Finally, the OLS regressions of the metric on the combined PDO/ENSO index were significant in ~1% (binary) and ~54% (fSCA) of the cases, exhibiting a negative slope in ~85% (binary) and ~100% (fSCA) of the cases. In conclusion, trend estimates are particularly robust to the way spikes are counted in the third metric, whereas the PDO/ENSO influence could become statistically significant in the case of fSCA data depending on how spikes are counted, which supports the notion that the PDO/ENSO is a driver of snow cover variability in the ecotone.

Varying the melt season start and end dates also indicated that cold and warm PDO/ENSO years can be significant predictors of snow cover for both the first and the second metric. The fSCA-based percent snow cover was significant at the 90% level in the initial analysis; however, had we used a slightly different start date of the snowmelt period, the differences would be significant at the 95% level (Fig. 9). Results are similar for the binary percent snow cover and the fSCA-based number of snow covered days, whereas binary-based number of snow covered days differences are almost always not significant (not shown). Importantly, all of these cold to warm differences remain positive, indicating that cold PDO/ENSO years exhibit more and longer lasting snow cover, which can be statistically significant depending on choice of season dates. In contrast to these PDO/ENSO results, long-term trends in the metrics remained statistically insignificant and small in magnitude for all combinations of season start and end dates for both the fSCA and the binary data (not shown).

4.4. Additional sources of uncertainty

In addition to spikes and the choice of snowmelt season start and end dates, several other sources of uncertainty may influence the study outcomes. Absolute validation of the snow cover product indicates accuracies of about 90% in general under clear skies (Hall & Riggs, 2007; Klein & Barnett, 2003); however retrieval accuracies deteriorate for evergreen forest land cover and are consistently worst for closed-canopy evergreen forests, where agreement with ground-based observations can be as low as 75–80% for some months (Simic, Fernandes, Brown, Romanov, & Park, 2004). There are inherent limitations of optical sensors in thick canopies because the canopy literally hides the snow (Rittger, Painter, & Dozier, 2013). The ecotone of interest here is exclusively in mountainous terrain that is covered with thick, closed-canopy evergreen forests. Additionally, errors are likely to be greatest when little snow is present, e.g. during transitional periods of accumulation and melt (Hall & Riggs, 2007; Klein & Barnett, 2003; Rittger et al., 2013). The choice of the 20% threshold for the ecotone to be deemed snow-free (Hall et al., 2010) can also influence the metrics. Passive optical and NIR remote sensing of snow affords relatively high spatial resolution (~500 m in this case); however, it can only be performed during daylight hours under clear skies. A related source of error likely to affect the snow algorithm in the ecotone are errors of omission and commission due to confusion with clouds, particularly at the edges of snow cover or on shadowed clouds that have a “yellow” spectrum (Riggs et al., 2006).

The cloud gap filling analysis uses data from up to three previous days, and thus each input image is a complex composite of up to four days of data. This can introduce additional uncertainty in the metrics, especially the timing of snowmelt. The detectable trends are smaller than 4 days/year (Fig. 8B–C), which illustrates that choosing to cloud gap fill is a compromise and can introduce large uncertainties. This motivates our choice to use only three days of previous observation to gap fill: assigning older observations to a given day can introduce larger uncertainties. Three days also was shown to be quite effective in reducing cloud gaps (Hall et al., 2010). Furthermore, a more sophisticated cloud gap filling technique with a spatial component is not recommended in a highly spatially heterogeneous terrain and a highly segmented ecotone such as our study area (Fig. 2). Finally, merging with MODIS *Aqua* data is also not recommended because of a missing channel compromising forest canopy corrections (Hall & Riggs, 2007).

Parallel analyses using binary and fSCA data allow comparison between the two products over the ecotone. Results indicate that binary data consistently show more snow cover and later snowmelt than fSCA data (Figs. 5–7). Detailed comparison of daily fSCA and binary data over the ecotone indicates that for 76% of snowmelt season days for which some binary pixels indicated snow, mean fSCA over those same pixels was less than 50%. Mean fSCA over binary pixels that indicated no snow was generally well under 50%. The binary algorithm is designed to detect snow if the pixel is more than 50% snow covered (Hall, Riggs, Salomonson, DiGirolamo, & Bayr, 2002); thus, fSCA and

binary data appear to be inconsistent over some pixels that are snow-covered according to the binary data. The binary algorithm is subject to errors of commission, which can explain this discrepancy (Rittger et al., 2013). fSCA data provide more information and are characterized by better validation statistics (Rittger et al., 2013). However, it is possible that fSCA data may be underestimating snow in the heavily forested ecotone, perhaps since the thick canopies obscure the snow. An NDVI-based enhancement of snow mapping in dense forests is applied to the MOD10A1.5 binary data set, but a correction for viewable area in thick canopies (e.g. Rittger et al., 2013, their Eq. (6)) is not applied to corresponding fSCA data (Riggs et al., 2006; Dorothy Hall, pers. comm.); this correction may help alleviate any underestimation problems in future studies. Rittger et al. (2013) analyzed Landsat data coarsened to 500 m resolution for MODIS product validation and observed that binary data introduces biases as expected in tree-free areas, i.e. underestimates when fSCA is smaller than ~45% and overestimates otherwise. However, under tree canopies, binary data indicated more snow than fSCA data for all fSCA greater than ~20%. Their result is consistent with our observation that fSCA in the forested hemlock-fir ecotone can indicate less than 50% snow cover when binary data indicate snow. Importantly for the conclusions presented here, in spite of underlying differences between the two data sets, trend estimates and relationships to the state of PDO/ENSO are virtually the same between binary and fSCA data.

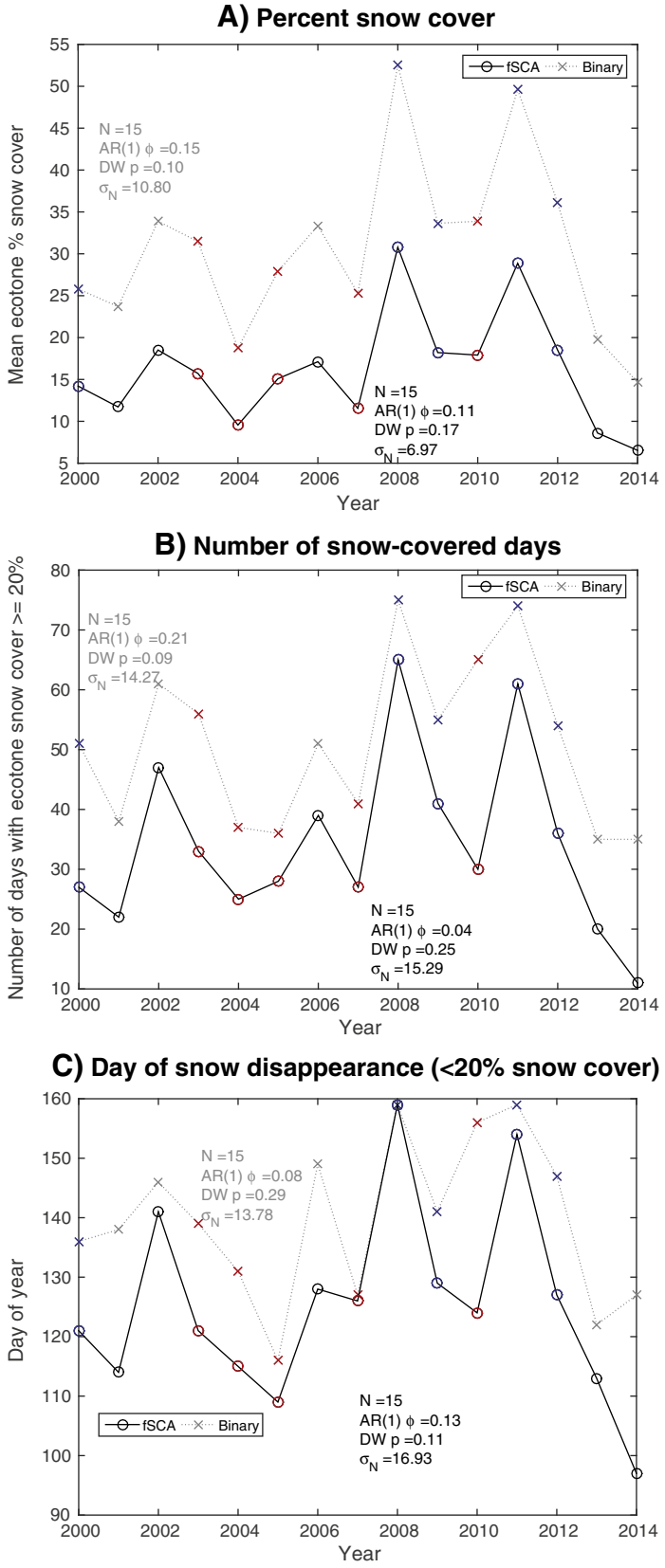

Retrievals based on physically-based spectral mixture analysis, such as the MODSCAG algorithm (Painter et al., 2009), are generally characterized by better validation statistics than the empirical NDSI-based products used here and are better able to map snow in transitional periods of accumulation and melt (Rittger et al., 2013). Snow-water equivalent remote-sensing retrievals are hydrologically and plant-relevant, but they have a very coarse resolution (Foster et al., 2005), thus they are less suitable to inform ecotone studies such as this one. Therefore, logical next steps of the analysis presented here include the use of the MODSCAG products (as long as the end-members are appropriate for the region), perhaps supported by a network of in-situ sensors that are able to resolve snow under clouds and thick canopies, as well as provide more variables and resolve spatial variability at very fine scales (Lundquist & Lott, 2008; Tyler et al., 2008).

Our analysis is specific to the time period studied (2000–2014) and the specific elevation range of the Oregon Western Cascades used to define the western hemlock-true fir ecotone. Different elevation ranges and different areas (e.g. to the north or south, or east of the Cascades ridge) may exhibit substantially different snow cover dynamics (Mote, 2006). In addition, we have focused on the snowmelt season only, rather than the entire water year. Importantly, the patterns identified cannot be assumed to be predictive for future years. Climate change projections indicate that Pacific Northwest temperatures will keep increasing (Mote & Salathé, 2010) and snow cover will likely substantially decrease, especially in at-risk areas, including in the Oregon Cascades (Nolin & Daly, 2006); such trends in snowpack parameters have already been observed over longer time periods than studied here (e.g. Mote, 2003; Mote et al., 2005). In addition, non-linearities are likely in the future due to feedbacks in the climate system. Additional variability in the snow cover metrics may be explained if the North Pacific Index (NPI) (Trenberth & Hurrell, 1994) is also considered (Mote, 2006).

Finally, the power analysis for trend detection (Fig. 8) assumes the data are not autocorrelated. While the MODIS time series indeed exhibits no autocorrelation (Fig. 7A–C), autocorrelation detection and estimation for such short time series is problematic (e.g. Bence, 1995; Schwarz, 2014). If positive autocorrelation is present, it will take longer to detect a trend. This is likely because the PDO tends to exhibit stable regime-

Fig. 7. Time series of the MODIS-derived hemlock-fir ecotone snow cover metrics for 2000–2014: (A) mean ecotone snow cover and (B) number of snow covered days during the snowmelt season (days of year 80 to 181) , and (C) the day of snow disappearance. Black solid curves with circles indicate fSCA-based analyses and gray dotted curves with crosses indicate binary-based analyses. Years classified as cold PDO/ENSO years are indicated with blue markers, whereas warm years are indicated with red markers. GLS regression statistics indicate very low R^2 values and non-significant slopes (not shown). Shown next to each time series are (black and gray, same as curve they refer to): N — the number of sample points, AR(1) ϕ, — the lag 1 autocorrelation, DW p — the p-value of the Durbin–Watson test for autocorrelation significance, and σ_N — the standard deviation of the residuals. (For interpretation of the references to color in this figure legend, the reader is referred to the web version of this article.)

Table 1
Medians of the ecotone snow cover metrics for cold and warm PDO and ENSO years. Metrics are calculated for the snowmelt season (days of year 80 to 181). Minimum and maximum values are given in parentheses after the median. The median differences for cold vs. warm years are also shown, and p-values of the Wilcoxon rank sum test for significance of these differences are provided in parentheses.

Type of metric	Cold years (2000, 2008, 2009, 2011, 2012)		Warm years (2003, 2004, 2005, 2007, 2010)		Difference (cold–warm years)	
Dataset used	fSCA	Binary	fSCA	Binary	fSCA	Binary
Mean ecotone percent snow cover	18.5 (14.2–30.8)	36.1 (25.8–52.5)	15.1 (9.6–17.9)	27.9 (18.7–33.9)	3.4 (0.056)	8.2 (0.095)
Number of snow covered days	41.0 (27–65)	55.0 (51–75)	28.0 (25–33)	41.0 (36–65)	13.0 (0.095)	14.0 (0.222)
Day of snow disappearance	129 (121–159)	147 (136–159)	121 (109–126)	131 (116–156)	8 (0.040)	16 (0.087)

like states lasting several years or decades (Climate Impacts Group, 2014b). Any gaps or discontinuities/level shifts in the data compromise our ability to create a self-consistent Climate Data Record (CDR, NRC (2004)) and detect climate change. Such level shifts would further increase the number of observations necessary to distinguish a long-term trend (Beaulieu et al., 2013; Weatherhead et al., 1998). Therefore, the number of years necessary to detect a trend presented in Fig. 8 should be treated as lower bounds. These results emphasize the need for long satellite missions that are meticulously calibrated. Continuity in order to avoid gaps and overlap of missions for cross-calibration are critical, as are algorithm consistency and advanced merging methods (e.g. Maritorena, d'Andon, Mangin, & Siegel, 2010; Maritorena & Siegel, 2005).

Ultimately, an improved understanding of the drivers of snowmelt at the western hemlock-true fir ecotone is an important input to dynamic species distribution modeling for this ecosystem. A mechanistic understanding of range expansion and contraction at species' distribution boundaries requires a detailed knowledge of both changes in the physical environment and changes in biotic response parameters related to species growth, establishment, decline and mortality (Breshears, Huxman, Adams, Zou, & Davison, 2008). It is likely that many more years of parallel observations are required to link snow trends to vegetation dynamics. Moreover, even at a high spatial resolution of 500 m, MODIS pixels remain very coarse compared to the fine spatial scale variability of various parameters relevant to seedling recruitment and survival (ground cover, slope, aspect, presence of nurse logs, proximity to large tree trunks), especially in mountainous terrain (Urban, Miller, Halpin, & Stephenson, 2000). Nevertheless, the detailed information on annual differences in snow metrics of direct relevance to plants is a valuable step towards a better understanding of these biophysical relationships.

5. Summary and conclusions

Snow is a dominant influence on the hydrology and ecology of western North American mountains; yet the dynamics of snowmelt at critical locations of these landscapes are rather poorly documented. Here we used the standard MODIS Terra snow cover products to investigate snow cover variability in the western hemlock-true fir ecotone of the Oregon Western Cascades during the snow depletion season. We developed several ecologically relevant snow cover metrics. The metrics were characterized by large interannual variability and no statistically significant linear trends during the 2000–2014 study period. Median differences of the metrics between warm and cold PDO/ENSO years were statistically significant depending on the choice of season start and end dates, indicating that the state of the PDO/ENSO is a driver of snow cover variability in the ecotone. However, large residual noise variance remained unexplained.

The short satellite record length available, the large noise levels in the data and the lack of significant trends necessitate estimation of the record length required to distinguish trends from noise. We generalized existing methods for power analyses of trend estimation that take into account autocorrelation. Our technique is fully described in Appendix A and can be applied to other data sets. The results indicated that at the level of noise exhibited by the MODIS record, at least ~30 years of uninterrupted observations are needed in order to distinguish trends of ± 0.5%/year in percent snow cover and ± 1 day/year in number of snow covered days or snow disappearance date. This is likely to be an underestimate due to possible autocorrelation in the data and the inevitable introduction of time series discontinuities due to the limited life-time of satellite missions. Smaller trends likely associated with climate change would take even longer to detect. These findings emphasize the need for continuous, high-quality satellite observations for the creation of Climate Data Records (CDRs), as well as enhanced ground measurement networks in closed canopy forests for algorithm development and validation.

Acknowledgments

This research was funded by an Associated Colleges of the South - Andrew W. Mellon Environmental Fellowship to T.R.L. and T.S.K. The University of Richmond School of Arts and Sciences also provided funding. Methodology for power analysis of trends was developed for analysis of ocean color data with funding from NASA Ocean Biology and Biogeochemistry grant #NNX13AC92G to T.S.K. Facilities and ancillary data were provided by the HJ Andrews Experimental Forest research program, funded by the National Science Foundation's Long-Term Ecological Research Program (DEB 1440409), US Forest Service Pacific Northwest Research Station, and Oregon State University. We are grateful to Anna Cabré for help with the GLS implementation, and to Claudie Beaulieu, Harish Vedantham, Geoffrey Henebry, and Annelen Kahl for useful discussions. NASA and NSIDC are hereby acknowledged for providing the MODIS snow cover data sets. Additional ancillary data were used to produce the maps of Figs. 2 and 3 as follows: vector boundaries of the Willamette National Forest (provided by the National Forest Service); vector boundary of the HJA (HJA LTER/OSU); the TIGER Census Oregon counties, populated areas, and state boundaries data; and the global self-consistent hierarchical high resolution shorelines (GSHHS) data set v2.2.0 coastlines data (Wessel & Smith, 1996). We are grateful to three anonymous reviewers for their comments which greatly improved the manuscript.

Appendix A. Power analysis of trend estimation via GLS regression

A.1. Generalized least squares (GLS) regression

Many time series are subject to autocorrelation, in which case an ordinary least squares (OLS) regression will underestimate the variance of the slope. The application of generalized least squares (GLS) regression to trend detection in time series that may exhibit first-order autocorrelation (AR(1)) is more appropriate (Beaulieu et al., 2013; Henson et al., 2010; Tiao et al., 1990; Weatherhead et al., 1998). For completeness, we provide a brief summary of GLS based on Beaulieu et al. (2013) and refs. therein. Consider a linear model

$$\mathbf{y} = \mathbf{Xb} + \mathbf{N} \tag{A1}$$

where $\mathbf{X}$ is the model's $n \times 2$ design matrix the first column of which contains 1's, and the second — the time variable, $\mathbf{b}$ is a 2×1 vector

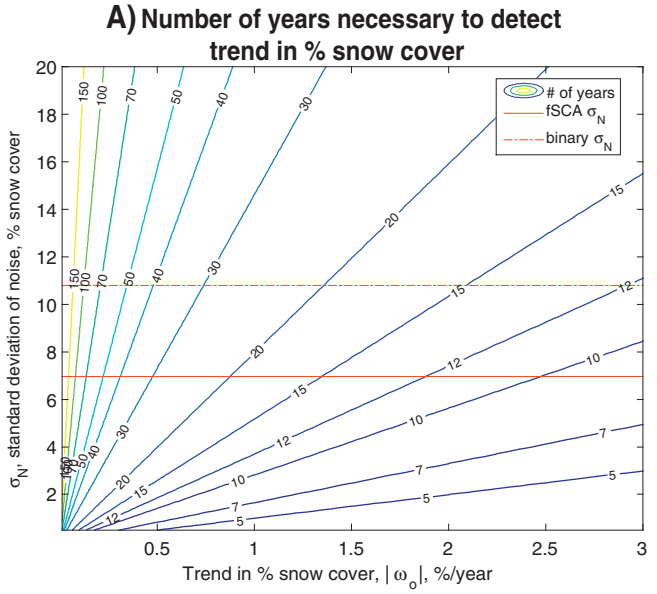

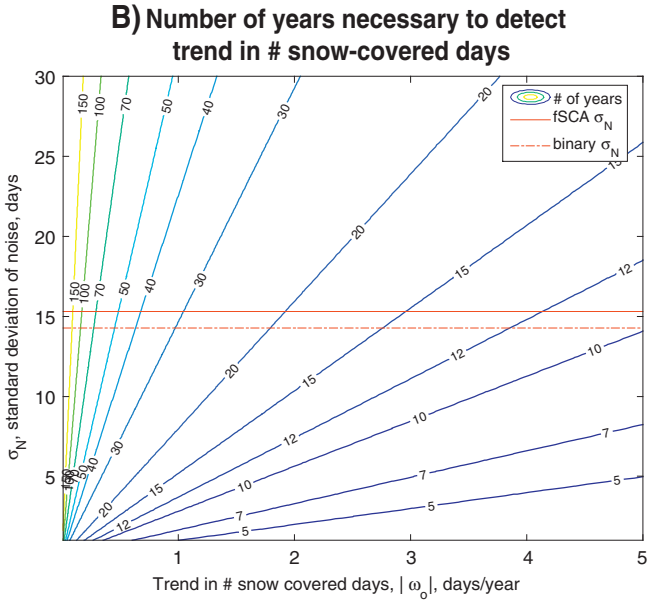

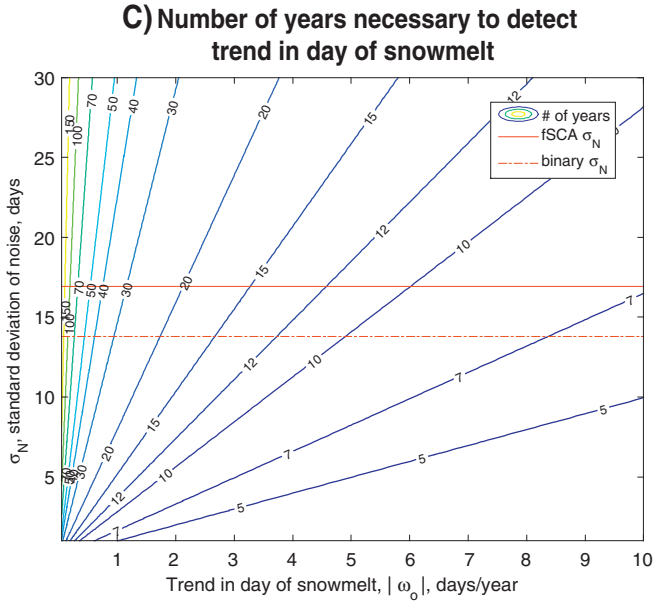

containing the intercept in b(1) and the slope in b(2), y is a $n \times 1$ vector of time series data and **N** is a $n \times 1$ vector of noise/residual terms (n is the number of samples). The slope represents the linear trend of the data and has the units of y per unit time. Assuming that the sampling is done in equal time intervals Δt and there is no missing data, the second column of **X** will be the vector [1,2,3,….n] $*$ Δt.

Autocorrelation of the noise terms **N** is expressed as the relationship $N_t = \phi N_{t-1} + e$ in the case of first order autocorrelation (Weatherhead et al., 1998), where ϕ is the first-order autocorrelation of the residuals. For this analysis, it is assumed that $|\phi| < 1$, i.e. the noise process is stationary (Weatherhead et al., 1998). Assuming an AR(1) process, the variance of the white noise σ_e^2 and the variance of the red noise, σ_N^2, are related via (Henson et al., 2010; Tiao et al., 1990; Weatherhead et al., 1998):

$$\sigma_N^2 = \frac{\sigma_e^2}{(1-\phi^2)}. \tag{A2}$$

The GLS estimators of the parameters in **b** from Eq. (A1) are given by:

$$\mathbf{b} = \left(\mathbf{X}'\mathbf{S}^{-1}\mathbf{X}\right)^{-1}\mathbf{X}\mathbf{S}^{-1}\mathbf{y} \tag{A3}$$

where the $n \times n$ covariance matrix **S** quantifies the autocorrelation of the residuals and its (i, j) element is constructed as follows:

$$S(i,j) = \sigma_N^2 \phi^{|i-j|}. \tag{A4}$$

The variance of the estimators of the slope and intercept in **b** is given by:

$$Var(\mathbf{b}) = \left(\mathbf{X}'\mathbf{S}^{-1}\mathbf{X}\right)^{-1}. \tag{A5}$$

Eq. (A5) is implicitly scaled by the variance of the noise σ_N^2 because the **S** matrix elements are multiplied by it (Eq. (A4)). We first estimate **N** using an OLS regression and ϕ is estimated as the autocorrelation of **N** at lag 1. The **S** matrix is then constructed, and **b**, **N** and ϕ are iteratively updated until convergence to less than 10^{-6} total percent difference in the elements of **b**.

A.2. Power analysis of GLS trend detection

Power analysis of the trend estimation refers to determining the number of observations necessary to distinguish a statistically significant trend from noise, with a given statistical power. This power analysis is based on deriving an expression for the variance of the slope (Eq. (A5)). In order to detect a linear trend that is significant at the 95% level, with statistical power of at least 90%, the following has

Fig. 8. Number of years, T^*, necessary to achieve a 90% probability to detect a 95% significant trend in the three ecotone melt season snow cover metrics analyzed: (A) percent ecotone snow cover, (B) number of snow covered days, and (C) day of snow disappearance. The absolute magnitude of the trend to detect is given on the x-axis, the amount of noise in the data (standard deviation) is on the y-axis, and the number of years necessary to detect the trend are indicated in colored and labeled contours. These are contours of Eq. (A9) with $\phi = 0$ (no autocorrelation) and $\Delta t = 1$ year (annual sampling). The standard deviation of the noise derived from real MODIS data is indicated with a red solid line for the fSCA-based data and with a red dash-dot line for the binary-based data. (For interpretation of the references to color in this figure legend, the reader is referred to the web version of this article.)

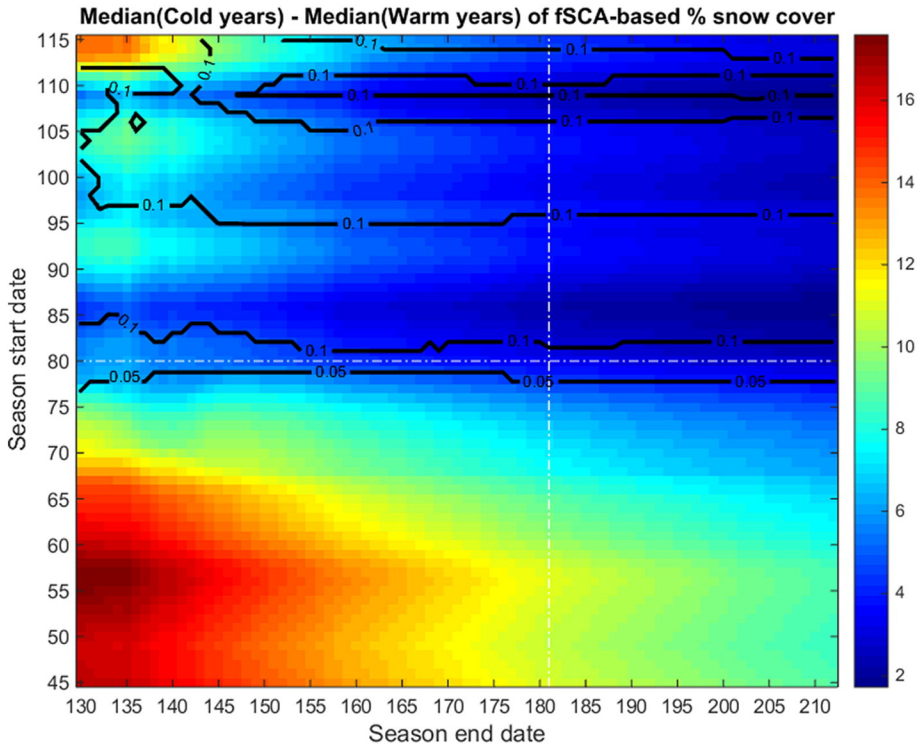

Fig. 9. Sensitivity of the difference in medians (and their significance) between cold and warm PDO/ENSO years to the choice of start (y-axis) and end (x-axis) dates of the melt season. The example is shown for fSCA-based percent snow cover during the melt season. The melt season used in the initial analyses is indicated by crossing dash-dot white lines. The color fill indicates the difference of medians (cold–warm), and the labeled contours indicate the p-value of the Wilcoxon rank sum test for a difference in medians. A value $p < 0.05$ indicates the two groups (warm vs. cold years) have significantly different medians at the 95% confidence level.

to be satisfied (Gerrodette, 1987; Tiao et al., 1990; Weatherhead et al., 1998):

$$\left|\frac{\omega}{\sigma_\omega}\right| \geq \left(z_{\alpha/2} + z_\beta\right) \tag{A6}$$

where ω is the trend to be detected, σ_ω is its standard deviation, and z_a is the value of a standard random normal variable such that the cumulative normal probability density function at z_a is $1 - a$ (i.e. the area under the tail beyond z_a is a). Here we take $\alpha = 0.05$ and $\beta = 0.1$, corresponding to probabilities of making a type I error (mistakenly identifying a trend that does not really exist) and type II error (missing a trend that really does exist), respectively (Gerrodette, 1987; Tiao et al., 1990). For the above values of α and β, the right hand side of Eq. (A6) equals about 3.25, closely corresponding to the value used in Tiao et al. (1990) and Weatherhead et al. (1998).

The minimum number of samples necessary to satisfy Eq. (A6) can be determined by assuming temporal sampling is occurring at regular intervals of time, Δt (Δt is the inverse of the sampling frequency). In that case the variance of the trend estimate can be solved for, either by assuming no autocorrelation and using ordinary least squares estimates (Gerrodette, 1987) or by using GLS regression and taking into account autocorrelation (Tiao et al., 1990; Weatherhead et al., 1998), as in the treatment here. Weatherhead et al. (1998) assume monthly sampling where the trend is expressed in per year units (i.e. $\Delta t = 1/12$ years) and demonstrate that an approximate analytical expression for the slope variance can be derived (better for $|\phi|$ not close to 1; see their Section A3). Generalizing their approach for any value of the sampling interval, we obtain the following *approximation*:

$$\sigma_\omega^2 \approx \sigma_e^2 \frac{12}{(1-\phi)^2 n(n^2-1)(\Delta t)^2} \tag{A7}$$

where ϕ is the lag 1 autocorrelation of the residual terms, n is the number of samples, and σ_ω^2 is the variance of the slope ω (the second element of the **b** vector in Eqs. (A1), (A3) and (A5)).

Substituting Eqs. (A2) and (A7) into Eq. (A6), and solving for n, we obtain n^*, the minimum *number of samples* required to detect a trend:

$$n^* \geq \left[\frac{3.25\sqrt{12}}{\Delta t}\frac{\sigma_N}{|\omega|}\sqrt{\frac{1+\phi}{1-\phi}}\right]^{2/3}. \tag{A8}$$

The above equation is valid as long as the given trend to be detected is expressed in the same time units as the sampling interval, and the sampling is assumed to be done at equal sampling intervals. In addition, the trend and the standard deviation of the noise need to be expressed in consistent units, either absolute units or percentages (Weatherhead et al., 1998).

If one wishes instead to determine the *number of time units* required to detect a given trend, T^*, rather than the number of samples n^*, Eq. (A8) is multiplied by Δt and becomes:

$$T^* \geq \left[\frac{3.25\sigma_N\sqrt{12\Delta t}}{|\omega|}\sqrt{\frac{1+\phi}{1-\phi}}\right]^{2/3}. \tag{A9}$$

A possible source of confusion needs to be clarified. Note that the factor of 12 in Eq. (A7) and subsequently Eqs. (A8) and (A9) appears because of the expression for the variance of the consecutive integers from 1 to n (Gerrodette, 1987). Additional factors of 1/12 will appear if the trend is expressed in per year units (time variable is in years) and sampling is monthly ($\Delta t = 1/12$ years), and these factors cancel in Eq. (A9) above, leading to the Weatherhead et al. (1998) result (their Eq. (3); they use a slightly different factor of 3.3 instead of 3.25 due to requiring $z_{\alpha/2} = 2$). Importantly, their n^* indicates the number of *years* required to detect the trend, *not* the number of samples, and the equation is specific to a situation where sampling frequency is

12 times per unit time interval. In other words, their n^* is denoted as T^* in the more general case treated here.

Finally, note that the autocorrelation coefficient ϕ and the variance of the noise σ_N^2 are specific to the sampling frequency. In other words, data sampled monthly is likely to have different autocorrelation and noise from data sampled daily or annually. Thus, analyses seeking to establish optimal sampling frequencies for a given trend detection need to take this dependence into account.

Appendix B. Supplementary data

Supplementary data to this article can be found online at http://dx.doi.org/10.1016/j.rse.2015.04.002.

References

Abatzoglou, J.T., Rupp, D.E., & Mote, P.W. (2014). Seasonal climate variability and change in the Pacific Northwest of the United States. *Journal of Climate*, *27*, 2125–2142.

Barnett, T.P., Adam, J.C., & Lettenmaier, D.P. (2005). Potential impacts of a warming climate on water availability in snow-dominated regions. *Nature*, *438*, 303–309.

Beaulieu, C., Henson, S.A., Sarmiento, Jorge L., Dunne, J.P., Doney, S.C., Rykaczewski, R.R., et al. (2013). Factors challenging our ability to detect long-term trends in ocean chlorophyll. *Biogeosciences*, *10*, 2711–2724. http://dx.doi.org/10.5194/bg-10-2711-2013.

Bence, J.R. (1995). Analysis of short time series: Correcting for autocorrelation. *Ecology*, 628–639.

Breshears, D.D., Huxman, T.E., Adams, H.D., Zou, C.B., & Davison, J.E. (2008). Vegetation synchronously leans upslope as climate warms. *PNAS*, *105*, 11591–11592.

Briles, C.E., Whitlock, C., Bartlein, P.J., & Higuera, P. (2008). Regional and local controls on postglacial vegetation and fire in the Siskiyou Mountains, northern California, USA. *Palaeogeography, Palaeoclimatology, Palaeoecology*, *265*, 159–169.

Cayan, D.R., Dettinger, M.D., Diaz, H.F., & Graham, N.E. (1998). Decadal variability of precipitation over western North America. *Journal of Climate*, *11*, 3148–3166.

Christopherson, R.W. (2012). *Geosystems: An introduction to physical geography*, *8/E*, Pearson/Prentice Hall.

Climate Impacts Group, University of Washington (2014a). Impacts of natural climate variability on Pacific Northwest climate. http://cses.washington.edu/cig/pnwc/clvariability.shtml (last accessed Dec. 26, 2014).

Climate Impacts Group, University of Washington (2014b). Comparing ENSO and PDO. http://cses.washington.edu/cig/pnwc/compensopdo.shtml (last accessed Dec. 26, 2014).

Dettinger, M.C., Cayan, D.R., Diaz, H.F., & Meko, D.M. (1998). North–south precipitation patterns in western North America on interannual-to-decadal timescales. *Journal of Climate*, *11*, 3095–3111.

Dingman, J.R., Sweet, L.C., McCullough, I., Davis, F.W., Flint, A., Franklin, J., et al. (2013). Cross-scale modeling of surface temperature and tree seedling establishment in mountain landscapes. *Ecological Processes*, *2*, 30.

Fay, A. R., & McKinley, G. A. (2013). Global trends in surface ocean pCO_2 from in situ data. *Global Biogeochemical Cycles*, *27*, 541–557. http://dx.doi.org/10.1002/gbc.20051.

Foster, J.L., Sun, C., Walker, J.P., Kelly, R., Chang, A., Dong, J., et al. (2005). Quantifying the uncertainty in passive microwave snow water equivalent observations. *Remote Sensing of Environment*, *94*(2), 187–203.

Fry, J., Xian, G., Jin, S., Dewitz, J., Homer, C., Yang, L., et al. (2011). Completion of the 2006 National Land Cover Database for the conterminous United States. *PE&RS*, *77*(9), 858–864.

Gedalof, Z., Peterson, D.L., & Mantua, N.J. (2004). Columbia River flow and drought since 1750. *Journal of the American Water Resources Association*, *40*(6), 1579–1592.

Gerrodette, T. (1987). A power analysis for detecting trends. *Ecology*, 1364–1372.

Gershunov, A., Barnett, T.P., & Cayan, D.R. (1999). North Pacific interdecadal oscillation seen as factor in ENSO-related North American climate anomalies. *EOS. Transactions of the American Geophysical Union*, *80*(3), 25–30. http://dx.doi.org/10.1029/99EO00019.

Gesch, D.B. (2007). The national elevation dataset. In D. Maune (Ed.), *Digital elevation model technologies and applications: The DEM users manual* (pp. 99–118) (2nd Edition). Bethesda, Maryland: American Society for Photogrammetry and Remote Sensing.

Gesch, D., Oimoen, M., Greenlee, S., Nelson, C., Steuck, M., & Tyler, D. (2002). The national elevation dataset. *Photogrammetric Engineering and Remote Sensing*, *68*(1), 5–11.

Hall, D.K., Foster, J.L., DiGirolamo, N., & Riggs, G.A. (2012). Snow cover, snowmelt timing and stream power in the Wind River Range, Wyoming. *Geomorphology*, *137*(1), 87–93. http://dx.doi.org/10.1016/j.geomorph.2010.11.011.

Hall, D.K., & Riggs, G.A. (2007). Accuracy assessment of the MODIS snow products. *Hydrological Processes*, *21*(12), 1534–1547.

Hall, D.K., Riggs, G.A., Foster, J.L., & Kumar, S.V. (2010). Development and evaluation of a cloud-gap-filled MODIS daily snow-cover product. *Remote Sensing of Environment*, *114*(3), 496–503.

Hall, D.K., Riggs, G.A., & Salomonson, V.V. (2001). *Algorithm Theoretical Basis Document (ATBD) for the MODIS snow and sea ice-mapping algorithms.* Greenbelt, MD: NASA Goddard Space Flight Center.

Hall, D.K., Riggs, G.A., Salomonson, V.V., DiGirolamo, N.E., & Bayr, K.J. (2002). MODIS snow-cover products. *Remote Sensing of Environment*, *83*, 181–194. http://dx.doi.org/10.1016/S0034-4257(02)00095-0.

Hall, D.K., Salomonson, V.V., & Riggs, G.A. (2006). MODIS/Terra snow cover daily L3 global 500 m grid. Boulder, Colorado USA: National Snow and Ice Data Center (Version 5. [Tile h09v04]).

Hamlet, A.F., & Lettenmaier, D.P. (1999). Columbia River streamflow forecasting based on ENSO and PDO climate signals. *Journal of Water Resources Planning and Management*, *125*, 333–341.

Hamlet, A.F., & Lettenmaier, D.P. (2007). Effects of 20th century warming and climate variability on flood risk in the western U.S. *Water Resources Research*, *43*(6).

Henson, S.A., Sarmiento, J.L., Dunne, J.P., Bopp, L., Lima, I., Doney, S.C., et al. (2010). Detection of anthropogenic climate change in satellite records of ocean chlorophyll and productivity. *Biogeosciences*, *7*, 621–640. http://dx.doi.org/10.5194/bg-7-621-2010.

IPCC (2013). Summary for policymakers. In T.F. Stocker, D. Qin, G. -K. Plattner, M. Tignor, S.K. Allen, J. Boschung, A. Nauels, Y. Xia, V. Bex, & P.M. Midgley (Eds.), *Climate CHANGE 2013: The physical science basis. Contribution of Working Group I to the Fifth Assessment Report of the Intergovernmental Panel on Climate Change*. Cambridge, United Kingdom and New York, NY, USA: Cambridge University Press.

Klein, A., & Barnett, A.C. (2003). Validation of daily MODIS snow maps of the Upper Rio Grande River Basin for the 2000–2001 snow year. *Remote Sensing of Environment*, *86*, 162–176.

Klein, A.G., Hall, D.K., & Riggs, G.A. (1998). Improving snow cover mapping in forests through the use of a canopy reflectance model. *Hydrological Processes*, *12*, 1723–1744.

Long, C.J., & Whitlock, C. (2002). Fire and vegetation history from the coastal rain forest of the western Oregon coast range. *Quaternary Research*, *58*, 215–225.

Lookingbill, T.R., Rocca, M.E., & Urban, D.L. (2011). Focused assessment of scale-dependent vegetation pattern. In A. Drew, Y. Wiersma, & F. Huettmann (Eds.), *Predictive Species and Habitat Modeling in Landscape Ecology* (pp. 111–138). New York: Springer Press.

Lookingbill, T.R., & Urban, D.L. (2005). Gradient analysis, the next generation: Towards more plant-relevant explanatory variables. *Canadian Journal of Forest Research*, *35*(7), 1744–1753.

Lundquist, J.D., & Lott, F. (2008). Using inexpensive temperature sensors to monitor the duration and heterogeneity of snow-covered areas. *Water Resources Research*, *44*, W00D16. http://dx.doi.org/10.1029/2008WR007035.

Mantua, N.J., Hare, S.R., Zhang, Y., Wallace, J.M., & Francis, R.C. (1997). A Pacific interdecadal climate oscillation with impacts on salmon production. *Bulletin of the American Meteorological Society*, *78*, 1069–1079.

Maritorena, S., d'Andon, O.H.F., Mangin, A., & Siegel, D.A. (2010). Merged satellite ocean color data products using a bio-optical model: Characteristics, benefits and issues. *Remote Sensing of Environment*, *114*(8), 1791–1804.

Maritorena, S., & Siegel, D.A. (2005). Consistent merging of satellite ocean color data sets using a bio-optical model. *Remote Sensing of Environment*, *94*(4), 429–440.

Moore, G.W.K., Holdsworth, G., & Alverson, K. (2002). Climate change in the North Pacific region over the past three centuries. *Nature*, *420*, 401–403.

Mori, A.S., Mizumachi, E., & Sprugel, D.G. (2008). Morphological acclimation to understory environments in Abies amabilis, a shade- and snow-tolerant conifer species of the Cascade Mountains, Washington, USA. *Tree Physiology*, *28*, 815–824.

Mote, P.W. (2003). Trends in snow water equivalent in the Pacific Northwest and their climatic causes. *Geophysical Research Letters*, *30*(12), 1601. http://dx.doi.org/10.1029/2003GL017258.

Mote, P.W. (2006). Climate-driven variability and trends in mountain snowpack in Western North America. *Journal of Climate*, *19*(23), 6209–6220.

Mote, P.W., Hamlet, A.F., Clark, M.P., & Lettenmaier, D.P. (2005). Declining mountain snowpack in western North America. *Bulletin of the American Meteorological Society*, *86*, 39–49.

Mote, P.W., & Salathé, E.P., Jr. (2010). Future climate in the Pacific Northwest. *Climatic Change*, *102*(1–2), 29–50.

Naik, P.K., & Jay, D.A. (2011). Distinguishing human and climate influences on the Columbia River: Changes in mean flow and sediment transport. *Journal of Hydrology*, *404*, 259–277.

National Research Council (NRC) (2004). *Climate data records from environmental satellites: Interim report.* Washington D.C., USA: The National Academies Press.

Nolin, A.W. (2010). Recent advances in remote sensing of seasonal snow. *Journal of Glaciology*, *56*, 1141–1150.

Nolin, A.W., & Daly, C. (2006). Mapping "at risk" snow in the Pacific Northwest. *Journal of Hydrometeorology*, *7*(5).

Painter, T.H., Rittger, K., McKenzie, C., Slaughter, P., Davis, R.E., & Dozier, J. (2009). Retrieval of subpixel snow covered area, grain size, and albedo from MODIS. *Remote Sensing of Environment*, *113*(4), 868–879.

Peng, J., Zhongbo, Y., & Gautam, M.R. (2013). Pacific and Atlantic Ocean influence on the spatiotemporal variability of heavy precipitation in the western United States. *Global and Planetary Change*, *109*, 38–45.

Raleigh, M.S., Rittger, K., Moore, C.E., Henn, B., Lutz, J.A., & Lundquist, J.D. (2013). Ground-based testing of MODIS fractional snow cover in subalpine meadows and forests of the Sierra Nevada. *Remote Sensing of Environment*, *128*, 44–57.

Riggs, G.A., Hall, D.K., & Salomonson, V.V. (2006). *MODIS snow products: User guide to collection 5.* Greenbelt, MD: NASA Goddard Space Flight Center.

Rittger, K., Painter, T.H., & Dozier, J. (2013). Assessment of methods for mapping snow cover from MODIS. *Advances in Water Resources*, *51*, 367–380.

Salomonson, V.V., & Appel, I. (2004). Estimating the fractional snow covering using the normalized difference snow index. *Remote Sensing of Environment*, *89*, 351–360.

Schwarz, C.J. (2014). Course notes for beginning and intermediate statistics, Ch. 16: Detecting trends over time. http://people.stat.sfu.ca/~cschwarz/CourseNotes/ (last accessed June 6, 2014).

Serreze, M.C., Clark, M.P., Armstrong, R.L., McGinnis, D.A., & Pulwarty, R.S. (1999). Characteristics of the western United States snowpack from snowpack telemetry (SNOTEL) data. *Water Resources Research*, *35*, 2145–2160.

Simic, A., Fernandes, R., Brown, R., Romanov, P., & Park, W. (2004). Validation of VEGETATION, MODIS, and GOES + SSM/I snow-cover products over Canada based on surface snow depth observations. *Hydrological Processes*, *18*(6), 1089–1104.

Stewart, I.T., Cayan, D.R., & Dettinger, M.D. (2005). Changes toward earlier streamflow timing across western North America. *Journal of Climate*, *18*(8), 1136–1155.

Tiao, G.C., Reinsel, G.C., Xu, D.M., Pedrick, J.H., Zhu, X.D., Miller, A.J., et al. (1990). Effects of autocorrelation and temporal sampling schemes on estimates of trend and spatial correlation. *Journal of Geophysical Research — Atmospheres*, *95*, 20507–20517. http://dx.doi.org/10.1029/JD095iD12p20507.

Trenberth, K.E., & Hurrell, J.W. (1994). Decadal atmosphere–ocean variations in the Pacific. *Climate Dynamics*, *9*, 303–319.

Trujillo, E., & Molotch, N.P. (2014). Snowpack regimes of the Western United States. *Water Resources Research*, *50*. http://dx.doi.org/10.1002/2013WR014753.

Tyler, S.W., Burak, S.A., McNamara, J.P., Lamontagne, A., Selker, J.S., & Dozier, J. (2008). Spatially distributed temperatures at the base of two mountain snowpacks measured with fiber-optic sensors. *Journal of Glaciology*, *54*(187), 673–679.

United States Global Change Research Program (USGCRP) (2000). *Water: The potential consequences of climate variability and change for the water resources of the United States. Report of the Water Sector Assessment Team of the National Assessment of the Potential Consequences of Climate Variability and Change.* Oakland, CA: Pacific Institute for Studies in Development, Environment, and Security, 151.

Urban, D.L., Miller, C., Halpin, P.N., & Stephenson, N.L. (2000). Forest gradient response in Sierran landscapes: The physical template. *Landscape Ecology*, *15*, 603–620.

Van Laningham, S., Duncan, R.A., Pisias, N.G., & Graham, D.W. (2008). Tracking fluvial response to climate change in, the Pacific Northwest: a combined provenance approach using Ar and Nd isotopic systems on fine-grained sediments. *Quaternary Science Reviews*, *27*, 97–517.

Weatherhead, E.C., Reinsel, G.C., Tiao, G.C., Meng, X.L., Choi, D.S., Cheang, W.K., et al. (1998). Factors affecting the detection of trends: Statistical considerations and applications to environmental data. *Journal of Geophysical Research — Atmospheres*, *103*, 17149–17161. http://dx.doi.org/10.1029/98jd00995.

Wessel, P., & Smith, W.H.F. (1996). A global, self-consistent, hierarchical, high-resolution shoreline database. *Journal of Geophysical Research*, *101*(B4), 8741–8743.

Wise, E.K. (2010). Spatiotemporal variability of the precipitation dipole transition zone in the western United States. *Geophysical Research Letters*, *37*, L07706.

Wolter, K. (1987). The Southern Oscillation in surface circulation and climate over the tropical Atlantic, Eastern Pacific, and Indian Oceans as captured by cluster analysis. *Journal of Climate and Applied Meteorology*, *26*, 540–558.

Wolter, K., & Timlin, M.S. (1993). Monitoring ENSO in COADS with a seasonally adjusted principal component index. *Proc. of the 17th Climate Diagnostics Workshop* (pp. 52–57). Norman, OK, NOAA/NMC/CAC, NSSL, Oklahoma Clim. Survey, CIMMS and the School of Meteor., Univ. of Oklahoma.

Wolter, K., & Timlin, M.S. (1998). Measuring the strength of ENSO events — How does 1997/98 rank? *Weather*, *53*, 315–324.

Zhang, Y., Wallace, J.M., & Battisti, D.S. (1997). ENSO-like interdecadal variability: 1900–93. *Journal of Climate*, *10*, 1004–1020.